



Single-layer chiral metasurface for circularly polarized light detection*

Xinjie SUN[‡], Xin HE[§], Zixin CAI, Xiang HAO[‡]

College of Optical Science and Engineering, Zhejiang University, Hangzhou 310027, China

E-mail: sunxj@zju.edu.cn; xinhe.wins@outlook.com; czx805660580@zju.edu.cn; haox@zju.edu.cn

Received Feb. 3, 2024; Revision accepted May 1, 2024; Crosschecked July 17, 2025

Abstract: Circular polarizers based on the metasurface suffer from a trade-off between the structural complexity and the polarization extinction ratio (ER). Herein, we present a single-layer chiral metasurface with strong circular dichroism. The structure turns a circularly polarized incident beam into a linearly polarized beam, achieving a high circular polarization ER. The operating wavelength of the proposed metasurface is tunable by changing the geometric parameters. The metasurface's localized surface plasmon resonances between structures ensure strong chiral optical effects. We further experimentally demonstrate the circular dichroism of the fabricated metasurface.

Key words: Optical metasurface; Polarization detection; Flat optical elements; Chiral metasurface
<https://doi.org/10.1631/FITEE.2400081>

CLC number: O43

1 Introduction

Polarization is critical for light. In particular, circularly polarized light (CPL) is widely used in holography (Wang Q et al., 2018; Wan et al., 2022), bioimaging, optical communication (Farshchi et al., 2011), and many other advanced optical technologies (Lin et al., 2004; Garcia et al., 2015). The detection of CPL has a high potential for the development of these optical technologies. Traditional optical CPL detection requires a quarter-wave plate (QWP), a linear polarizer (LP), and other mechanically rotating components. This causes substantial losses in sensitivity and

resolution in light detection. However, the progress in optical metasurfaces provides opportunities for ultra-thin CPL detection and manipulation.

Optical metasurfaces are artificial electromagnetic media structured on the subwavelength scale that exhibit unprecedented properties. Over the past few years, optical metasurfaces have been employed for the design and fabrication of optical elements and systems with abilities that surpass the performance of conventional optical elements (Pendry et al., 2006; Soukoulis and Wegener, 2010; Yu et al., 2011; Frese et al., 2019).

Specifically, for polarization applications, a three-dimensional (3D) chiral optical metasurface was first proposed to differentiate the handedness of CPL (Hentschel et al., 2017), performing a wider regulation bandwidth and a higher circular polarization extinction ratio (ER). For example, the gold helix achieves an ER of 20 over a wide wavelength range (Gansel et al., 2010). The spiral-type ramp-shaped metamaterial (Rajaei et al., 2019) and the L-shaped metallic strip can also achieve optical chirality (Dietrich et al., 2012). Three-dimensional structures achieve high ERs and broad bandwidths. However, the fabrication

[‡] Corresponding author

[§] The two authors contributed equally to this work

* Project supported by the National Key Research and Development Program of China (No. 2022YFB3206000), the Fundamental Research Funds for the Central Universities (No. 2022QZJH29), the National Natural Science Foundation of China (Nos. 92050115 and 42201336), and the Zhejiang Provincial Natural Science Foundation of China (No. LZ21F050003)

ORCID: Xinjie SUN, <https://orcid.org/0000-0003-0463-9074>; Xin HE, <https://orcid.org/0000-0002-5843-0332>; Zixin CAI, <https://orcid.org/0009-0001-2076-5997>; Xiang HAO, <https://orcid.org/0000-0002-3931-6884>

© Zhejiang University Press 2025

of these complicated nanostructures has a high requirement for the equipment and the fabrication procedure, which is a fatal limitation to mass production.

With the development of nanotechnology, planar lithography techniques, such as photolithography and electron-beam lithography, have become mature, and the multi-layer metasurface dominates the research on artificial nanostructures for CPL detection. Multi-layer metasurfaces realize circular dichroism by rotating components of each layer or combining diverse metasurfaces to form a 3D chiral structure (Zhao Y et al., 2012; Wang ZJ et al., 2016; Yun et al., 2017; Bai et al., 2019; Gorkunov et al., 2020; Cen et al., 2022; Zhao X et al., 2022). The ER of a multi-layer metasurface can reach 35 in experiments (Basiri et al., 2019). However, the multi-layer metasurface also suffers from fabrication challenges. For example, aligning vertically adjacent layers always requires a complex fabrication procedure involving multiple lithography and film deposition steps.

Single-layer structures can also be chiral and present circular dichroism, providing an alternative that has a simplified fabrication procedure. However, they always suffer from relatively low ERs in simulations (below 20) (Li et al., 2015; Zhang et al., 2017; Ma et al., 2018).

To resolve this dilemma, we develop a single-layer chiral metasurface that performs better circular dichroism and demonstrate it both in theory and through experiments. The operating wavelength of the proposed metasurface is tunable by changing the geometric parameters. The mechanism of high ER is explored through the simulated electric field and the component analysis of the transmitted light. In addition, we fabricate the structure and verify the circular dichroism of the proposed single-layer chiral metasurface in experiments. We further analyze the reason for the difference between the simulation and the experiment.

2 Design and simulation

We applied the Jones matrix to characterize the polarization state conversion through the given interface. The transmission matrix of the conversion between a circularly polarized base and a linearly polarized base is described as

$$\mathbf{T}_{\text{cir}} = \begin{pmatrix} t_{\text{RR}} & t_{\text{RL}} \\ t_{\text{LR}} & t_{\text{LL}} \end{pmatrix} = \frac{1}{2} \begin{pmatrix} (t_{\text{xx}} + t_{\text{yy}}) + i(t_{\text{yx}} - t_{\text{xy}}) & (t_{\text{xx}} - t_{\text{yy}}) - i(t_{\text{xy}} + t_{\text{yx}}) \\ (t_{\text{xx}} - t_{\text{yy}}) + i(t_{\text{xy}} + t_{\text{yx}}) & (t_{\text{xx}} + t_{\text{yy}}) - i(t_{\text{xy}} - t_{\text{yx}}) \end{pmatrix}, \quad (1)$$

where R and L in the subscripts represent the right circularly polarized (RCP) and the left circularly polarized (LCP) light, respectively. The first and second subscripts denote the polarizations of the transmitted light and incident light, respectively. Circular dichroism arises when $T_{\text{L}} \neq T_{\text{R}}$. The transmittance of LCP and RCP incidence (T_{L} and T_{R}) is given by

$$T_{\text{L}} = T_{\text{LL}} + T_{\text{RL}} = |t_{\text{LL}}|^2 + |t_{\text{RL}}|^2, \quad (2)$$

$$T_{\text{R}} = T_{\text{RR}} + T_{\text{LR}} = |t_{\text{RR}}|^2 + |t_{\text{LR}}|^2. \quad (3)$$

For any single-layer metasurface with in-plane mirror symmetry, the Jones matrix is diagonalized so that the cross-polarization transmission coefficient $t_{\text{xy}} = t_{\text{yx}} = 0$ (Menzel et al., 2010). This indicates that no polarization state conversion occurs in this structure, and the circular dichroism is zero since $T_{\text{L}} = T_{\text{R}}$. To break the structural symmetry and create the dichroism, we employed the chiral metasurface, which is not consistent with its mirror structure by any azimuthal angle. We define the circular polarization ER as follows to quantify the circular dichroism of the structure:

$$\text{ER} = T_{\text{R}} / T_{\text{L}}. \quad (4)$$

Fig. 1 shows our single-layer metasurface circular polarizer, which is composed of gold nano-gratings and a nanorod array. A right-handed circular polarizer selectively transmits RCP light and converts it into linearly polarized light (LPL). The unit cell of the metasurface (Fig. 1b) is designed as a chiral structure to generate strong circular dichroism via asymmetric metallic plasmonic distribution. The period of the array is sub-wavelength to avoid high-order diffraction. SiO₂ is used as the substrate. A 5-nm-thick Cr adhesive layer lies between the substrate and the gold layer. The gratings are along the *y*-axis, while the rectangular nanorods rotate 45° from the gratings and are repeated along the *x*- and *y*-axis. Remarkably, the handedness of the metasurface polarizer is switchable,

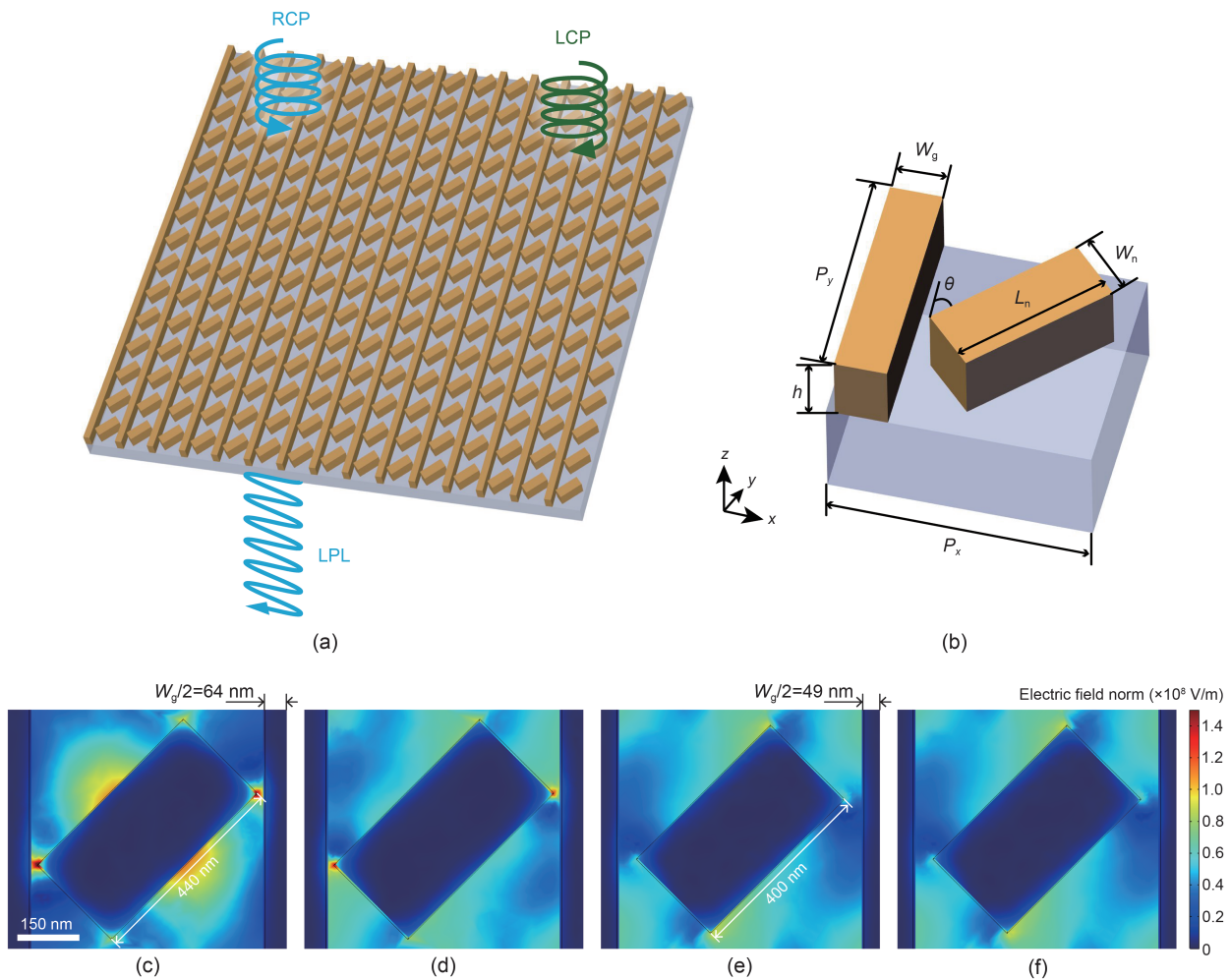


Fig. 1 Schematic illustration of the single-layer metasurface circular polarizer: (a) overview of the proposed metasurface; (b) schematic of a single meta-molecule; (c, e) simulated electric field for left circularly polarized (LCP) illumination of the metasurface with 840 nm operating wavelength; (d, f) simulated electric field for right circularly polarized (RCP) illumination of the metasurface with 840 nm operating wavelength. The periods of meta-molecules are P_x and P_y along the x -axis and y -axis, respectively. Nano-gratings have a width W_g . Rectangular nanorods rotate by $\theta=45^\circ$ with respect to nano-gratings and have a width W_n and a length L_n , and their thickness is h . (c) and (d) correspond to $L_n=440$ nm and $W_g=128$ nm, and (e) and (f) correspond to $L_n=400$ nm and $W_g=98$ nm. LPL: linearly polarized light. References to color refer to the online version of this figure

depending on the selective absorption of the polarization component. When LCP absorption dominates ($\theta=45^\circ$), our metasurface acts as a right-handed polarizer, whereas it converts to a left-handed polarizer when $\theta=-45^\circ$. Notably, there is nearly no difference in the simulation results between the right-handed and left-handed polarizers. Therefore, this paper only presents and analyzes the results of the right-handed polarizer.

We chose this single-layer chiral structure since its localized surface plasmon resonance (LSPR) distribution is polarization-dependent; this phenomenon

in turn triggers strong circular dichroism. To understand the underlying mechanism, we simulated the near-field electric distribution around the metasurface under illumination light with different circular polarization states (Figs. 1c and 1d). For the LCP illumination shown in Fig. 1c, a strong electric field appears in the middle of the long side of the rectangular nanorods, which results in high absorption. In contrast, for the RCP illumination (Fig. 1d), the electric field is weaker but has a more uniform distribution. In this way, our metasurface allows selective polarization transmission and conversion.

Notably, the performance of our metasurface is closely related to the geometric parameters. When these parameters deviate from the optimal values (with L_n decreased by 40 nm and W_g decreased by 30 nm compared to those in Figs. 1c and 1d), the intensity of LSPR around the nanorod is dramatically weakened as shown in Figs. 1e and 1f, and the ER decreases from 34 to 14. These two electric fields, shown in Figs. 1e and 1f, under illuminations with different handedness, do not differ significantly, thereby impairing the circular dichroism of our metasurface. Based on the proposed structure, the optimal values of geometric parameters of four operating wavelengths are shown in Table 1. We intentionally kept all minimum distances between the nano-grating and the nanorod above 20 nm to guarantee that the pattern is producible

using electron beam lithography (EBL). For quantitative analysis, we further calculated their corresponding ERs using full-wave simulations (Fig. 2). In Figs. 2a–2d, the solid black and dashed lines represent the transmittance of LCP and RCP incidence, respectively, and the solid red lines represent the ER. In general, the ER values are consistent with the theoretical prediction. The transmittance of a specific-handed CPL can be close to zero, whereas its orthogonal component maintains a higher transmittance, realizing an ER peak around the desired operating wavelength. For example, as shown in Fig. 2c, when the wavelength is 1300 nm, the transmittance of LCP and RCP light is 0.006 and 0.300, respectively, resulting in a peak ER value of 50. A similar trend is also visible in Figs. 2a–2d. Remarkably, in addition to the four operating

Table 1 Key parameters of the metasurface for simulation

| Operating wavelength (nm) | Simulated ER | P_x (nm) | P_y (nm) | W_g (nm) | W_n (nm) | L_n (nm) | h (nm) |
|---------------------------|--------------|------------|------------|------------|------------|------------|----------|
| 720 | 15 | 640 | 600 | 128 | 180 | 440 | 200 |
| 840 | 34 | 840 | 720 | 143 | 310 | 610 | 200 |
| 1300 | 50 | 1350 | 980 | 135 | 500 | 720 | 350 |
| 1580 | 18 | 1550 | 1200 | 155 | 600 | 1050 | 400 |

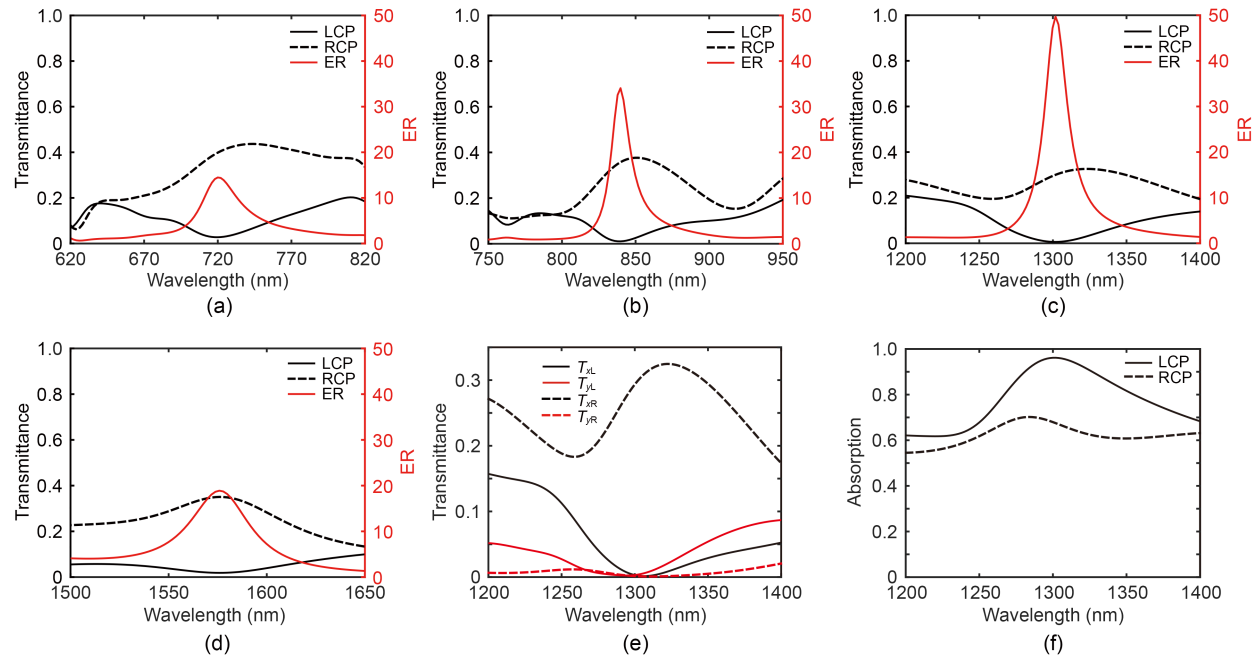


Fig. 2 Simulation results as a function of operating wavelength: (a–d) transmittance of LCP and RCP light and extinction ratio (ER) of the metasurfaces working at 720 nm (a), 840 nm (b), 1300 nm (c), and 1580 nm (d); (e) transmittance of linear polarization when the incident light is circularly polarized; (f) absorption spectra for LCP and RCP incidences. References to color refer to the online version of this figure

wavelengths mentioned above, this model can effectively cover the visible to near-infrared range (700–1600 nm).

We investigated the optical response of our metasurface operating at 1300 nm in detail. Fig. 2e shows the transmittance of linearly polarized components when the incident light is circularly polarized. The x -polarized component has a higher transmittance compared to the y -polarized component, which is determined by the orientation of the nano-gratings in the metasurface (Basiri et al., 2019). In particular, at a wavelength of 1300 nm, the transmittance of x -polarized light is 0.3, whereas that of y -polarized light is almost zero. The planar chirality of the metasurface causes cross-polarization conversion to differentiate the transmittance of LCP and RCP incidence. For the incident light, 96% of the LCP component is absorbed (Fig. 2f). Therefore, our metasurface polarizer converts the RCP incidence to LPL at high efficiency but absorbs the LCP component.

3 Fabrication and results

To demonstrate our metasurface circular polarizer on a challenging target for fabrication, we opted for 720 nm as the shortest operating wavelength (Table 1). We fabricated a right-handed array on a silica substrate. A 5-nm-thick Cr adhesive layer followed by a 200-nm-thick gold layer was deposited on the silica substrate by a high vacuum evaporation system (ei-5z). The pattern was fabricated by EBL (RAITH VOYAGER). Fig. 3a shows the scanning electron microscope (SEM) images of the fabricated metasurface.

To characterize the transmittance of the fabricated metasurface, we used a custom spectrometer integrated into a microscope (Fig. 3b). The unpolarized light from a halogen tungsten lamp was converted by a combination of an LP and a QWP into the CPL to illuminate the sample. The transmitted light was collected by a microscope and then detected by a spectrometer. A flip mirror was set between the lenses to reflect the light into the camera as needed.

The measured results are shown in Fig. 3c. In brief, the transmittance of LCP light is lower than that of RCP light, which is consistent with the simulation results. The measured transmitted spectra also

perform the discrimination of different handedness illuminations, as expected. The measured peak ER reaches 2.5. This value is lower than that in simulation, mainly due to the deviation during the multi-step fabrication. Due to the limitation of fabrication accuracy, to keep a clear gap between the nano-grating and the nanorod, SEM was used to measure the gap as being enlarged to 80 nm during actual processing instead of 37 nm as the design. This is mainly because the manufacturing accuracy of EBL is not high enough. To demonstrate the impact of manufacturing errors, we adjusted the geometric parameters of the metasurface operating at 720 nm, as shown in Table 1, to match the measured parameters of the fabricated metasurface in Fig. 3a. Fig. 3d illustrates the simulation results, confirming the influence of manufacturing errors on the metasurface's performance, as indicated by a decrease in the peak ER from 14.5 in Fig. 2a to 6.2 in Fig. 3d. Additionally, inaccurate fabrication led to a shift in the peak wavelength. However, it is feasible to fabricate 37 nm gaps and achieve a metasurface that better conforms to the designed parameters using higher-precision equipment (Devlin et al., 2016). We were also aware that the roughness of the nano-gratings was up to 5 nm, which also decreased the device performance. However, the peak position was maintained, which validates our overall design.

4 Conclusions

We designed and fabricated a single-layer chiral metasurface structure for CPL distinction. The metasurface converts a specific-handed CPL into LPL and absorbs the orthogonal component. The single-layer chiral structure holds the promise of a high ER. It can work from 700 nm to 1600 nm by tuning the geometric parameters. Four examples at 720 nm, 840 nm, 1300 nm, and 1580 nm are shown in this paper. The ability to convert one specific-handed CPL into LPL stems from the nano-gratings and the chiral plasmonic structure. Our experimental results demonstrate the circular dichroism of the proposed chiral metasurface. However, there is still room for improvement during the fabrication process. Our study holds the promise of a high ER, tunable operation, simple fabrication, and integration. It can be applied to fiber

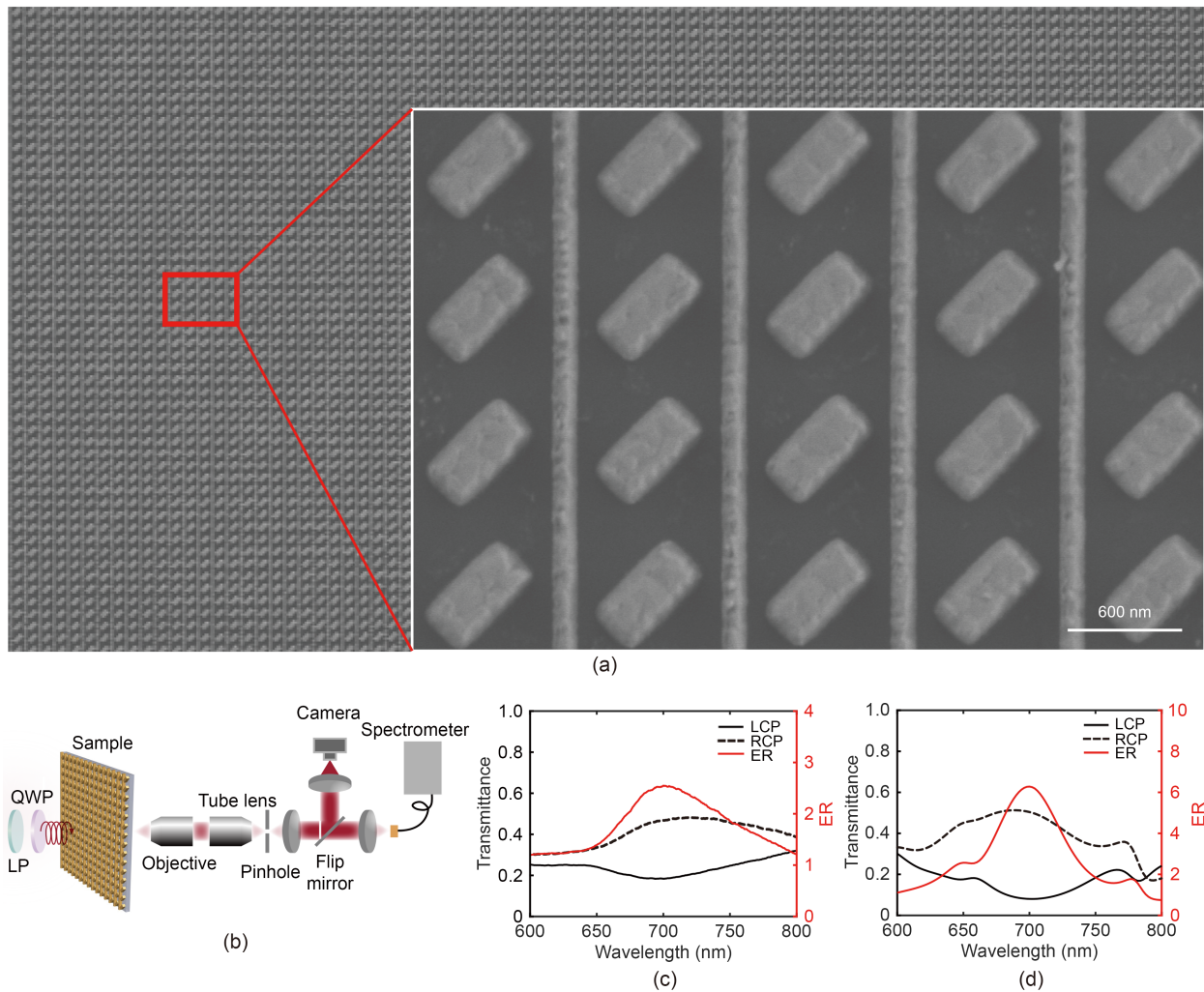


Fig. 3 Fabrication and characterization of the single-layer metasurface circular polarizer: (a) scanning electron microscope (SEM) images of the right-handed fabricated metasurface; (b) schematic of the experimental setup; (c) measured results of the fabricated metasurface; (d) simulation results of the metasurface adjusting its geometric parameters according to the fabricated metasurface. LP: linear polarizer; QWP: quarter-wave plate. References to color refer to the online version of this figure

optics, chip-integrated systems for quantum computing, polarimetric detectors, and emission and sensing applications for CPL.

Contributors

Xinjie SUN, Xin HE, and Xiang HAO designed the research. Xinjie SUN processed the data, performed the theoretical analysis and the measurement of the sample, and drafted the paper. Xinjie SUN and Xin HE fabricated the samples. Zixin CAI helped organize the paper. Xinjie SUN, Xin HE, and Xiang HAO revised and finalized the paper.

Acknowledgments

This work was partially carried out at the Micro-Nano Fabrication Center of Zhejiang University. We also thank the

Westlake Center for Micro/Nano Fabrication for facility support and technical assistance.

Conflict of interest

Xiang HAO is a corresponding expert of *Frontiers of Information Technology & Electronic Engineering*, and he was not involved with the peer review process of this paper. All the authors declare that they have no conflict of interest.

Data availability

Data underlying the results presented in this paper are not publicly available at this time but may be obtained from the authors upon reasonable request.

References

Bai J, Wang C, Chen XH, et al., 2019. Chip-integrated

- plasmonic flat optics for mid-infrared full-Stokes polarization detection. *Photon Res*, 7(9):1051-1060. <https://doi.org/10.1364/PRJ.7.001051>
- Basiri A, Chen XH, Bai J, et al., 2019. Nature-inspired chiral metasurfaces for circular polarization detection and full-Stokes polarimetric measurements. *Light Sci Appl*, 8:78. <https://doi.org/10.1038/s41377-019-0184-4>
- Cen MJ, Wang JW, Liu JX, et al., 2022. Ultrathin suspended chiral metasurfaces for enantiodiscrimination. *Adv Mater*, 34(37):2203956. <https://doi.org/10.1002/adma.202203956>
- Devlin RC, Khorasaninejad M, Chen WT, et al., 2016. Broadband high-efficiency dielectric metasurfaces for the visible spectrum. *Proc Natl Acad Sci USA*, 113(38):10473-10478. <https://doi.org/10.1073/pnas.1611740113>
- Dietrich K, Lehr D, Helgert C, et al., 2012. Circular dichroism from chiral nanomaterial fabricated by on-edge lithography. *Adv Mater*, 24(44):321-325. <https://doi.org/10.1002/adma.201203424>
- Farshchi R, Ramsteiner M, Herfort J, et al., 2011. Optical communication of spin information between light emitting diodes. *Appl Phys Lett*, 98(16):162508. <https://doi.org/10.1063/1.3582917>
- Frese D, Wei QS, Wang YT, et al., 2019. Nonreciprocal asymmetric polarization encryption by layered plasmonic metasurfaces. *Nano Lett*, 19(6):3976-3980. <https://doi.org/10.1021/acs.nanolett.9b01298>
- Gansel JK, Wegener M, Burger S, et al., 2010. Gold helix photonic metamaterials: a numerical parameter study. *Opt Expr*, 18(2):1059-1069. <https://doi.org/10.1364/OE.18.001059>
- Garcia NM, de Erasquin I, Edmiston C, et al., 2015. Surface normal reconstruction using circularly polarized light. *Opt Expr*, 23(11):14391-14406. <https://doi.org/10.1364/OE.23.014391>
- Gorkunov MV, Antonov AA, Kivshar YS, 2020. Metasurfaces with maximum chirality empowered by bound states in the continuum. *Phys Rev Lett*, 125(9):093903. <https://doi.org/10.1103/PhysRevLett.125.093903>
- Hentschel M, Schäferling M, Duan XY, et al., 2017. Chiral plasmonics. *Sci Adv*, 3(5):1602735. <https://doi.org/10.1126/sciadv.1602735>
- Li W, Coppens ZJ, Besteiro LV, et al., 2015. Circularly polarized light detection with hot electrons in chiral plasmonic metamaterials. *Nat Commun*, 6:8379. <https://doi.org/10.1038/ncomms9379>
- Lin SS, Yemelyanov KM, Pugh EN, et al., 2004. Polarization enhanced visual surveillance techniques. *IEEE Int Conf on Networking, Sensing and Control*, p.216-221. <https://doi.org/10.1109/ICNSC.2004.1297437>
- Ma ZJ, Li Y, Li Y, et al., 2018. All-dielectric planar chiral metasurface with gradient geometric phase. *Opt Expr*, 26(5):6067-6078. <https://doi.org/10.1364/OE.26.006067>
- Menzel C, Rockstuhl C, Lederer F, 2010. Advanced Jones calculus for the classification of periodic metamaterials. *Phys Rev A*, 82(5):053811. <https://doi.org/10.1103/PhysRevA.82.053811>
- Pendry JB, Schurig D, Smith DR, 2006. Controlling electromagnetic fields. *Science*, 312(5781):1780-1782. <https://doi.org/10.1126/science.1125907>
- Rajaei M, Zeng JW, Albooyeh M, et al., 2019. Giant circular dichroism at visible frequencies enabled by plasmonic ramp-shaped nanostructures. *ACS Photon*, 6(4):924-931. <https://doi.org/10.1021/acsp Photonics.8b01584>
- Soukoulis CM, Wegener M, 2010. Optical metamaterials—more bulky and less lossy. *Science*, 330(6011):1633-1634. <https://doi.org/10.1126/science.1198858>
- Wan WP, Yang WH, Ye S, et al., 2022. Tunable full-color vectorial meta-holography. *Adv Opt Mater*, 10(22):2201478. <https://doi.org/10.1002/adom.202201478>
- Wang Q, Plum E, Yang QL, et al., 2018. Reflective chiral meta-holography: multiplexing holograms for circularly polarized waves. *Light Sci Appl*, 7:25. <https://doi.org/10.1038/s41377-018-0019-8>
- Wang ZJ, Jia H, Yao K, et al., 2016. Circular dichroism metamirrors with near-perfect extinction. *ACS Photon*, 3(11):2096-2101. <https://doi.org/10.1021/acsp Photonics.6b00533>
- Yu NF, Genevet P, Kats MA, et al., 2011. Light propagation with phase discontinuities: generalized laws of reflection and refraction. *Science*, 334(6054):333-337. <https://doi.org/10.1126/science.1210713>
- Yun JG, Kim SJ, Yun H, et al., 2017. Broadband ultrathin circular polarizer at visible and near-infrared wavelengths using a non-resonant characteristic in helically stacked nano-gratings. *Opt Expr*, 25(13):14260-14269. <https://doi.org/10.1364/OE.25.014260>
- Zhang F, Pu MB, Li X, et al., 2017. All-dielectric metasurfaces for simultaneous giant circular asymmetric transmission and wavefront shaping based on asymmetric photonic spin-orbit interactions. *Adv Funct Mater*, 27(47):1704295. <https://doi.org/10.1002/adfm.201704295>
- Zhao X, Li ZC, Cheng JQ, et al., 2022. Realization of maximum optical intrinsic chirality with bilayer polyatomic metasurfaces. *Opt Lett*, 47(18):4814-4817. <https://doi.org/10.1364/OL.469518>
- Zhao Y, Belkin MA, Alù A, 2012. Twisted optical metamaterials for planarized ultrathin broadband circular polarizers. *Nat Commun*, 3:870. <https://doi.org/10.1038/ncomms1877>